

LA-UR-18-27596 (Accepted Manuscript)

Nonlinear resonant ultrasound spectroscopy of stress corrosion cracking in stainless steel rods

Hogg, Stephen M
Anderson, Brian E
Le Bas, Pierre-Yves
Remillieux, Marcel

Provided by the author(s) and the Los Alamos National Laboratory (2019-07-18).

To be published in: NDT & E International

DOI to publisher's version: 10.1016/j.ndteint.2018.12.007

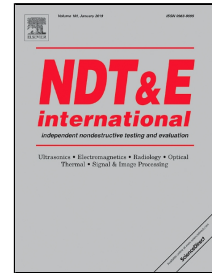
Permalink to record: <http://permalink.lanl.gov/object/view?what=info:lanl-repo/lareport/LA-UR-18-27596>

Disclaimer:

Los Alamos National Laboratory, an affirmative action/equal opportunity employer, is operated by Triad National Security, LLC for the National Nuclear Security Administration of U.S. Department of Energy under contract 89233218CNA000001. By approving this article, the publisher recognizes that the U.S. Government retains nonexclusive, royalty-free license to publish or reproduce the published form of this contribution, or to allow others to do so, for U.S. Government purposes. Los Alamos National Laboratory requests that the publisher identify this article as work performed under the auspices of the U.S. Department of Energy. Los Alamos National Laboratory strongly supports academic freedom and a researcher's right to publish; as an institution, however, the Laboratory does not endorse the viewpoint of a publication or guarantee its technical correctness.

Accepted Manuscript

Nonlinear resonant ultrasound spectroscopy of stress corrosion cracking in stainless steel rods



Stephen M. Hogg, Brian E. Anderson, Pierre-Yves Le Bas, Marcel C. Remillieux

PII: S0963-8695(18)30584-X
DOI: 10.1016/j.ndteint.2018.12.007
Reference: JNDT 2069
To appear in: *NDT and E International*
Received Date: 08 October 2018
Accepted Date: 14 December 2018

Please cite this article as: Stephen M. Hogg, Brian E. Anderson, Pierre-Yves Le Bas, Marcel C. Remillieux, Nonlinear resonant ultrasound spectroscopy of stress corrosion cracking in stainless steel rods, *NDT and E International* (2018), doi: 10.1016/j.ndteint.2018.12.007

This is a PDF file of an unedited manuscript that has been accepted for publication. As a service to our customers we are providing this early version of the manuscript. The manuscript will undergo copyediting, typesetting, and review of the resulting proof before it is published in its final form. Please note that during the production process errors may be discovered which could affect the content, and all legal disclaimers that apply to the journal pertain.

20 **Abstract:** Stainless steel containers are susceptible to stress corrosion cracking (SCC) under
21 certain stress and corrosion conditions. Nonlinear ultrasonic techniques are very sensitive to the
22 early presence of damage, more so than linear techniques. Nonlinear Resonant Ultrasound
23 Spectroscopy (NRUS) is used here to measure a nonlinear shift in the resonance frequency due
24 to a cumulative amount of SCC. Steel rods are immersed in a heated magnesium chloride
25 solution and removed after different exposure times. NRUS measurements are conducted using
26 the fundamental longitudinal mode of vibration. Rods exposed longer generally have a larger
27 resonance frequency shift and are therefore more nonlinear. Thus NRUS might offer a means of
28 detecting a cumulative SCC damage in a sample.

29

30 **Keywords:** stress corrosion cracking; nonlinear resonant ultrasound spectroscopy;
31 nondestructive evaluation; nondestructive testing

32

33 **1. Introduction**

34 Nondestructive evaluation (NDE) methods are needed to characterize damage on 304L stainless
35 steel nuclear storage casks to prevent leakage of radioactivity from cracks [1]. One type of
36 damage of interest is Stress Corrosion Cracking (SCC). SCC occurs when a stress exists,
37 including residual stresses from welding, and the metal is in a corrosive environment (including
38 airborne chlorides) [1]. These conditions results in an electrochemical reaction that makes the
39 metal susceptible to cracking [1]. SCC is most likely to occur in the Heat Affected Zone (HAZ).
40 HAZs are regions of residual stresses created during the welding process. The intense heat of the
41 welding process causes the material properties and grain boundaries within the HAZ to be
42 changed [2]. This affects the strength of the metal and degrades the metal's capacity to resist
43 corrosion, meaning SCC is more likely. SCC can be small enough that visual techniques and
44 linear NDE techniques cannot detect it very easily. Linear NDE techniques often rely on a
45 reflection of sound off of damage (e.g. cracks and delaminations), but if the crack is too small or
46 is a closed crack with the crack surfaces in contact, then no reflection will occur and the crack
47 will be transparent to the incident wave. NDE techniques based on nonlinear acoustics, on the
48 other hand, are well suited to detect closed cracks because surfaces in contact with one another
49 vibrate nonlinearly when excited with sufficiently high amplitude [3]. The full extent of the
50 crack can therefore be measured with nonlinear NDE techniques. Linear techniques also
51 sometimes monitor the ultrasonic attenuation as increases in attenuation are known to be a sign
52 of damage in a sample. As will be discussed in this paper, nonlinear ultrasonics are more
53 sensitive to the presence of damage than the measured changes in attenuation (or quality factor).

54 Young's modulus is strain independent in linear elasticity, but in damaged materials it
55 depends on the strain experienced by the material. If we strike a damaged steel rod with a
56 hammer harder and harder, a progressively lower frequency tone will be emitted due to nonlinear
57 effects and the apparent material softening (i.e., drop of the elastic constants) [4]. Higher
58 longitudinal strains lower the Young's modulus according to Remillieux *et al.* [5],

$$59 \quad E(x) = E_0 \left[1 - \alpha_E \epsilon_{xx}^{\max}(x) \right], \quad (1)$$

60 where $E(x)$ is amplitude dependent Young's Modulus, E_0 is the undamaged Young's modulus of
61 the bulk material, and ϵ_{xx}^{\max} is the maximum strain measured in the longitudinal direction during a
62 longitudinal mode of vibration. Here α_E is a nonclassical nonlinear elastic parameter that has
63 been correlated with inhomogeneity. For instance, freshly milled stainless steel will have a very
64 low, close to zero, α_E . A sedimentary rock, such as sandstone, will have a much larger α_E .
65 Damaged materials will also exhibit a finite value for α_E . Remillieux *et al.* obtained α_E from the
66 amplitude dependence of the resonance frequencies of longitudinal modes and then showed that
67 α_E is different when it is obtained from amplitude dependent shifts of torsional mode resonance
68 frequencies. Prior to the work of Remillieux *et al.* researchers typically only measured the
69 amplitude dependence of longitudinal modes frequencies of resonance.

70 Nonlinear Resonant Ultrasound Spectroscopy (NRUS) is a technique used to measure α_E
71 [6]. NRUS measures the amplitude dependence of a particular sample's resonance frequency. A
72 swept sine wave excitation signal is used to extract the resonance frequency. The amplitude of
73 the excitation signal is then increased several times and the resulting resonance frequency noted

74 each time. A downward shift in the resonance frequency with increasing strain amplitude is often
75 encountered for damaged materials as the elastic moduli soften (as implied in Eq. (1)). The peak
76 strain at the resonance frequency peak is also extracted. The slope of a plot of the relative
77 frequency shift as a function of strain determines α_E for the sample [6].

78 NRUS was initially developed to characterize the inherent nonlinearity of natural rock
79 samples such as sandstone, soapstone, and granite [7]. It has been applied to characterize damage
80 in inherently linear materials that normally exhibit no frequency shift in their undamaged state,
81 but that do exhibit a frequency shift in their damaged state, such as fatigue damage in copper and
82 creep damage in stainless steel [8,9]. It has been applied to characterize thermal damage in
83 concrete and damage in bone because even though these materials exhibit a frequency shift in
84 their undamaged state, the shift increases further due to the presence of damage [10-12].

85 Various nonlinear acoustic techniques have been used to detect and characterize SCC.
86 Ohara *et al.* developed the Subharmonic Phased Array to image SCC using surface acoustic
87 waves [13,14]. Dynamic Acousto-Elastic Testing employs a low frequency pump and higher
88 frequency probe technique that was used by Rivière *et al.* to extract α_E and additional nonlinear
89 parameters [15]. Ohara *et al.* used NRUS to partially locate SCC by analyzing the measured α_E
90 from different resonance modes based on whether the mode had a strain node or antinode at the
91 location of the SCC [16]. An experiment by Morlock *et al.* used nonlinear Rayleigh surface
92 waves to characterize SCC on four samples with different amounts of SCC [17]. Morlock *et al.*
93 applied different amounts of stress to two sets of samples while they were exposed to sodium
94 thiosulfate. Within these sets of samples, some were exposed for 1 week while the others were

95 exposed for 3 weeks. They reported an increase in the second harmonic amplitude for the
96 samples will higher stress and with longer exposure time, though they found that the second
97 harmonic amplitude initially decreased with the first week of exposure (relative to a sensitized
98 state) and then returned to its original value after 3 weeks of exposure. Anderson *et al.* used the
99 Time Reversed Elastic Nonlinearity Diagnostic to explore the depth dependence of SCC near
100 welds [18]. The majority of the nonlinear acoustic techniques were applied to a single sample for
101 proof of concept of the technique's ability to detect SCC rather than being applied to a set of
102 samples with progressive damage. A book reviewing nonlinear ultrasonic techniques was very
103 recently published, which includes a description of the Subharmonic Phased Array, Dynamic
104 Acousto-Elastic Testing, NRUS, Rayleigh waves, and the Time Reversed Elastic Nonlinearity
105 Diagnostic [19].

106 The purpose of this paper is to determine whether the measured α_E using NRUS correlates
107 with exposure time (likely corresponding to an overall increase in SCC damage) in 304L
108 stainless steel rod samples, and if so, what that functional dependence is. Samples are placed in a
109 hot magnesium chloride (MgCl_2) bath for varying lengths of time to induce SCC. Here we excite
110 only the fundamental longitudinal mode of rod samples because that is the type of resonance
111 mostly commonly used in NRUS experiments. It will be shown that α_E in progressively damaged
112 samples does increase with the corrosive environment exposure time and that NRUS can be used
113 to quantify the cumulative amount of damage by measuring α_E . Thus here we are measuring α_E
114 instead of the beta parameter associated with second harmonic generation as was used by
115 Morlock *et al.* and we exposed more samples to a corrosive environment for different lengths of

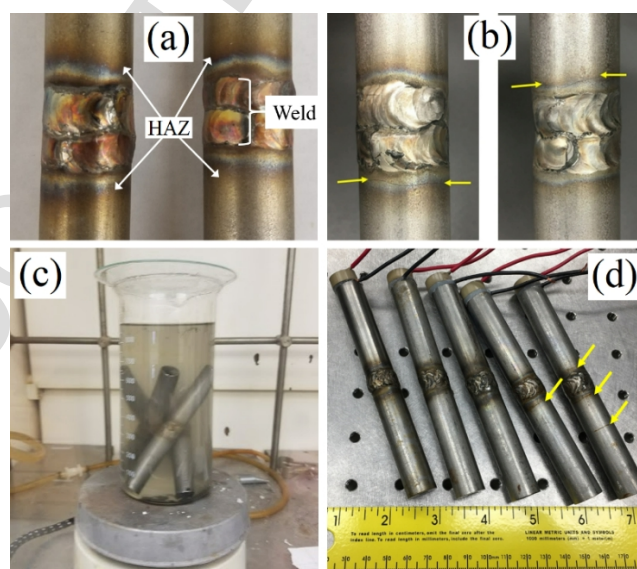
116 time that they did. The purpose of this study is not to provide a direct forecast of the α_E expected
117 for a given exposure time of SCC accumulation in storage casks since the corrosion process for
118 storage casks is much slower than the one used here. Rather this paper indicates that there is an
119 exponential increase in α_E with exposure time for the samples studied here and we suggest that
120 an exponential increase would be expected for other systems, albeit with different exponential fit
121 parameters.

122

123 **2. Sample creation**

124 Samples of 304L stainless steel having a weld and a cylindrical shape were created. The simple
125 cylindrical geometry ensures that individual modes may be identified and excited. The weld
126 provides a HAZ where SCC would most likely develop. No external stress is applied to the
127 samples. The actual samples were created by welding two 6.35 cm (2.5 in.) length pieces to
128 create 12.7 cm (5 in.) long samples. The weld material is 308 stainless steel, the same weld
129 material used for nuclear storage casks. Figure 1(a) displays a photograph of two virgin samples
130 with the weld and HAZ identified. Visually the samples appear to be welded similarly. Figure
131 1(b) displays a photograph of two damaged samples with visible cracks identified by the arrows.
132 Prior to inducing damage in the samples, the fundamental longitudinal resonance frequencies
133 were measured to determine a measure of the consistency in the samples. The mean frequency
134 value was 19.49 kHz and the frequencies ranged from 19.42 kHz to 19.55 kHz, implying that the
135 samples were made in a fairly consistent manner.

136 To induce SCC, samples are placed in a hot, corrosive environment to accelerate the
137 development rate of cracking. The environment consists of a 42% $MgCl_2$ solution created by
138 mixing tap water with anhydrous $MgCl_2$. The 1 L beaker used to contain the solution is
139 maintained at the 500 mL mark. The solution is heated to 80° C using a hot plate for the duration
140 of the exposure of the rods to the solution (see Fig. 1(c)). The high temperature causes
141 evaporation, necessitating refilling the beaker. Evaporation is minimized by using a watch glass
142 to mostly cover the beaker, allowing evaporated water to condense on the watch glass and drip
143 back down into the solution. Only water is needed to restore the $MgCl_2$ -water ratio, since only
144 the water evaporates. Adding additional $MgCl_2$ causes oversaturation. When samples are
145 removed, $MgCl_2$ and water are added to maintain the 42% solution since some salt adheres to the
146 removed rods and needs to be replaced. Twelve samples are initially placed in the solution and
147 one is taken out every two days. Figure 1(d) displays a photograph of 5 of the samples with
148 varying degrees of exposure and visible cracks identified by arrows. Any residual salt that
149 collected on the rods was washed off.



150

151 Fig. 1. (color online) (a) Close up photograph of 2 of the samples prior to exposure. Also depicted are the
152 weld region and the Heat Affected Zone (HAZ). (b) Close up photograph of 2 of the damaged samples with
153 cracks identified by arrows. (c) Photograph of some of the samples in the hot magnesium chloride solution
154 in a fume hood. (d) Photograph of five of the samples with differing amounts of exposure and cracking
155 (identified by the arrows).

156

157 3. Experimental setup

158 NRUS experiments are controlled and data are acquired using custom LabVIEW software. A
159 stepped sine wave excitation signal is output from a National Instruments PXI-5406 FGEN card
160 (16-bit resolution and 40 MHz sampling frequency). Each step consists of a sine wave that lasts
161 for the duration of the specified 50 ms ring-up and 50 ms acquisition times. This allowed for
162 avoiding the transient ring up and to record approximately 800 cycles of time during the steady
163 state portion of the sample excitation. This signal is amplified using a Tabor Electronics
164 amplifier, model 9400 with a fixed 50× gain. The amplified signal is sent to a cylindrical, APC
165 International piezoelectric transducer of type 851, with dimensions 15.7 mm diameter by 6.4 mm
166 thickness. The response of the sample is measured by a Polytec PSV-400 Scanning Laser
167 Doppler Vibrometer (SLDV), whose output is digitized with a National Instruments PXIe-5122
168 digitizer (14-bit resolution and 100 MHz sampling frequency). The laser is shined on the flat end
169 of the cylinder opposite to the piezoelectric transducer (PZT).

170 The frequency range of the stepped sine wave signal is selected to excite the first
171 longitudinal mode of vibration of the sample. This sample, of mass m and length L excited by
172 wavenumber k can be modeled as having a mass loaded end (with the piezoelectric transducer as
173 the mass load, m_b) and a free end,

174
$$\tan(kL) = - (m/m_b)kL. \quad (2)$$

175 This transcendental equation is used to predict the longitudinal resonances [20,21]. Samples of
176 length 12.7 cm (5 in.) and diameter 1.59 cm (5/8 in.) are found to have longitudinal modes that
177 are sufficiently separated from torsional and flexural mode frequencies that were estimated by
178 assuming free-free bar boundary conditions (experimental measures of the modal frequencies of
179 all three types of modes were in decent agreement).

180 NRUS data have a frequency resolution of 0.2 Hz. The frequency range used depends on
181 the resonance frequency of the sample under test. Relatively undamaged samples have a
182 frequency range that is slightly wider than the full width at half maximum span of frequencies.
183 More damaged samples require a wider frequency range that extends further below the sample's
184 resonance frequency, because the frequency shift is greater in damaged samples. The sample
185 exposed for the longest time, which is expected to have the most damage, is measured from 14.8-
186 15.4 kHz while the undamaged sample was measured from 18.2-18.5 kHz. These frequency
187 ranges correspond to the span necessary to capture the resonance frequency peaks at each of the
188 drive amplitudes. The NRUS measurements utilize excitation voltage levels of 10V-100V in
189 increments of 10V output from the amplifier to the transducer.

190

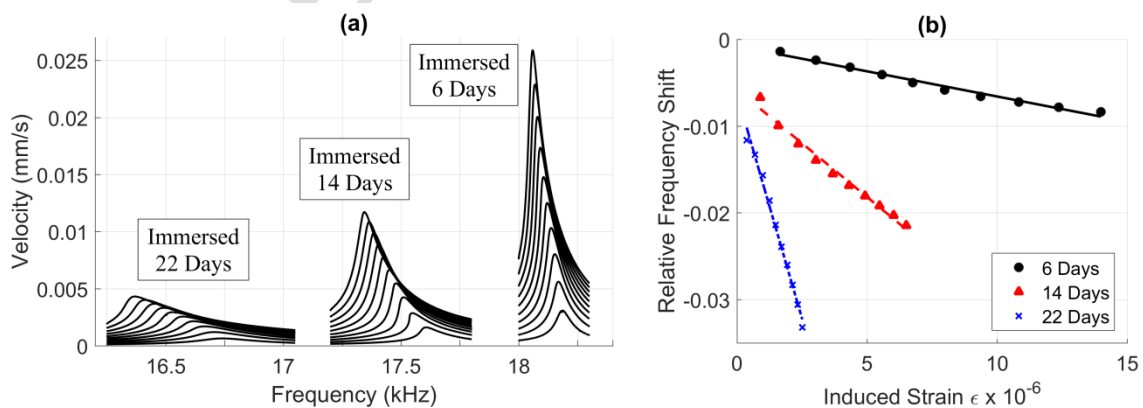
191 **4. Results and discussion**

192 Figure 2(a) displays sample NRUS measurements from samples exposed for 6, 14, and 22 days.
193 Once the NRUS data is obtained, a parabolic peak-finding algorithm is used to carefully identify
194 the peaks of the resonance curves, including the frequency at which the peak occurs and the

195 amplitude of the peak. The measured peak amplitudes and resonance frequencies are exported to
 196 MATLAB to apply linear curve fitting in order to extract the α_E of the sample. The relative
 197 frequency shift is defined as

$$198 \quad \frac{\Delta f}{f_0} = \frac{(f_i - f_0)}{f_0}, \quad (3)$$

199 where f_i is the measured resonance frequency (obtained from the peak-finding algorithm) at the
 200 i th excitation amplitude and f_0 is the lowest amplitude resonance frequency measured. The
 201 strain for each resonance curve is calculated by dividing the peak velocity measured (obtained
 202 from the peak-finding algorithm) by the sample's longitudinal wave speed [5]. Note that this
 203 estimation of the strain is an approximation based on a homogeneous sample. Our samples are
 204 not homogenous due to the weld material in the middle and because these samples have localized
 205 cracking in them. It has been recently shown that the nonlinearity obtained using NRUS is an
 206 average estimation of the local nonlinearity driven by the local strain field over the entire sample
 207 [22]. The strain, ϵ , reported should represent values close to those actually experienced in these
 208 rods, particularly where the damage appears to be most prevalent, near the weld towards the
 209 middle of the sample where the strain is expected to be the largest.



210

211 Fig. 2. (color online) (a) Sample nonlinear resonant ultrasound spectroscopy plots from three samples
 212 exposed to 80°C magnesium chloride for 6, 14, and 22 days. (b) Relative frequency shift as a function of
 213 induced strain, ϵ , for the three samples whose results were plotted in (a). Included are trend lines which
 214 indicate the linear fits to the data.

215
 216 The relative frequency shift values are plotted as a function of the strain and analyzed in
 217 MATLAB using a least-squares linear fit to extract the slope of the data. The absolute value of
 218 the slope is the measured α_E . Figure 2(b) displays three sets of relative frequency shift data as a
 219 function of strain for the NRUS results displayed in Fig. 2(a) along with the linear fit to each
 220 data set. The measured α_E are 5.80×10^2 , 2.47×10^3 , and 1.03×10^4 , respectively. The respective
 221 coefficient of correlation, R , values were 0.992, 0.992, and 0.996.

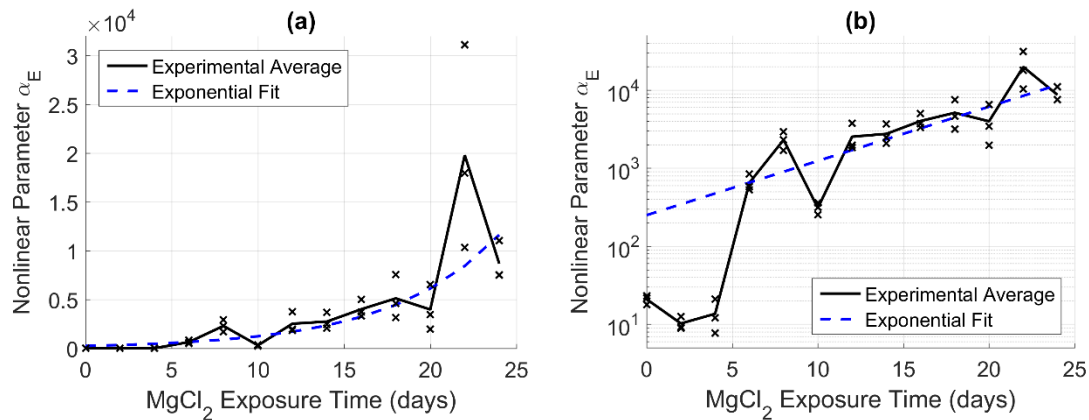
222 Table 1. Results given for experiments conducted on 13 samples. The quality factor and Young's modulus
 223 are measured during a low level excitation. There is a general increase in α_E as the days exposed to MgCl_2
 224 increases.

Days Exposed	Quality Factor	Young's Modulus (GPa)	Max $\frac{\Delta f}{f_0}$ ($\times 10^{-3}$)	Max Strain ($\mu\epsilon$)	α_E	R
0	455	175	0.48	25.9	21.7	0.953
2	460	176	0.31	23.9	9.26	0.911
4	473	175	0.44	24.7	7.71	0.807
6	298	171	8.37	14.0	581	0.992
8	138	162	10.5	4.20	1690	0.999
10	294	162	5.56	11.6	3140	0.974
12	152	161	10.3	5.23	1970	0.997
14	182	163	21.5	6.50	2480	0.992
16	166	164	21.5	5.70	3710	0.994
18	234	158	22.1	6.50	2170	0.999

20	242	166	13.4	7.05	1960	0.938
22	74.6	149	33.2	2.51	10300	0.996
24	103	121	26.8	2.40	7500	0.977

226

227 The process outlined above is followed for 13 samples. Table 1 displays the measured
 228 quality factor for the lowest amplitude excitation resonance curve, the effective Young's
 229 modulus calculated from the sound speed in Eq. (2) and the lowest amplitude resonance
 230 frequency (assuming the mass of the rods was unchanged), the maximum frequency shift
 231 measured at the highest excitation level, the maximum strain induced, the measured α_E , and the
 232 R of the linear fit for each sample. The quality factor changes by a factor of 6.2 and the Young's
 233 modulus by a factor of 1.5, whereas α_E changes by more than 3 orders of magnitude, by up to a
 234 factor of 1300, demonstrating the much higher sensitivity of a nonlinear technique over linear
 235 techniques that rely on changes to the quality factor and/or the Young's modulus.



236

237 Fig. 3. The measured nonlinearity parameter, α_E , as a function of exposure time for the samples tested. (a)
 238 linear and (b) logarithmic scales. The “x” symbols represent each of three measurements on each sample
 239 and the solid line represents their average values. The dashed line represents the exponential fit of Eq. (4).

240

241 Figure 3 plots α_E as a function of time exposed to MgCl_2 . NRUS was conducted on each
242 sample 3 times (the “×” marks on the figure) and the average of the 3 results is depicted by the
243 solid line. It should be noted that while there is not a consistent monotonic increase, α_E appears
244 to increase exponentially with a longer exposure time. A least-squares empirical fit to the data,
245 between 6 days and 24 days, with an exponential function yielded

$$246 \quad \alpha_E = 250e^{0.16t}, \quad (4)$$

247 where t is time in days, with $R = 0.828$. Other fit functions (i.e. linear, quadratic, and power
248 law) did not provide as high of a R value. The use of a large set of samples exposed to MgCl_2
249 may provide for a better empirical fit α_E versus exposure time, but the purpose of this study was
250 to show that α_E increases with exposure time for a set of samples. In the application of NRUS to
251 structures of interest, the rate of growth in α_E versus exposure time would likely be different
252 because the corrosion conditions would likely be different and the condition of the residual stress
253 on the structures would be different. Prior to 6 days there was essentially no change in α_E . The
254 α_E for the virgin sample is actually slightly higher than the α_E for the samples exposed for 2 and
255 4 days, though the α_E for all three of these samples is very low, suggesting that no damage was
256 induced until 6 days of exposure. Note that the fit parameters will almost certainly be specific to
257 the rods and corrosive environment used here.

258 Several assumptions were made that could account for discrepancies in the data. It was
259 assumed that the welds on the rods were identical with identical rod geometries. Differences in
260 the welding process for each sample can result in different residual stress conditions. Different

261 residual stresses in the rods could easily result in damage induced at different rates since the
262 difference in HAZs (e.g. greater variability in grain boundaries) would mean that certain rods
263 would be more susceptible to SCC. It was also assumed that the piezoelectric transducers are the
264 same and that they were bonded to the samples in the same manner. If this assumption weren't
265 true, each bar would have different excitation amplitudes, resulting in different strain
266 measurements, which affects the measured α_E . One advantage of NRUS measurements is that
267 the determination of α_E is independent of changes in the linear elastic modulus and the mass of
268 the sample, meaning that baseline measurements of samples before and after corrosion
269 treatments are not as imperative as they would be for several other NDE techniques.

270

271 5. Conclusion

272 Twelve stainless steel samples have been exposed to hot magnesium chloride for different
273 lengths of time ranging from 2 days to 24 days to induce Stress Corrosion Cracking (SCC) in an
274 accelerated manner. Nonlinear Resonant Ultrasound Spectroscopy (NRUS) was used to measure
275 the amplitude dependence of the first longitudinal resonance frequency of the samples. The
276 nonlinear parameter, α_E , was extracted from the relative shifting of the resonance frequencies,
277 measured as a function of assumed strain levels. It was found that SCC can be induced in a
278 relatively fast manner using lower temperatures than typically used in the literature [23]. It was
279 also found that while there is not a perfect monotonic increasing trend, there still is a general
280 exponential trend between exposure time and the measured α_E , which suggests that the NRUS
281 results are likely correlated with the cumulative degree of SCC in a sample. Differences in the

282 data are thought to be due to differences in the welding process when the samples were created.
283 Given the assumptions made, the trend shown in Fig. 3 indicates that higher quantities of SCC
284 damage exhibit larger nonlinear shifts in resonance frequency. Application of this process to
285 detecting SCC in storage casks, or other systems, would require determining the relationship of
286 α_E to exposure time for that specific system, though an exponential increase in α_E with time is
287 expected based on the results shown here.

288

289 **Acknowledgements**

290 Funding provided by the U.S. Department of Energy, Nuclear Energy University Program
291 through Integrated Research Project Award Number DE-NE0008442 and a subcontract from Los
292 Alamos National Laboratory to Brigham Young University (BYU). Additional support provided
293 by the BYU College of Physical and Mathematical Sciences.

294 **References**

- 295 [1] Meyer RM, Hanson B, Sorenson K. A review of NDE methods for detecting and
296 monitoring of atmospheric SCC in dry cask storage canister for used nuclear fuel. NACE
297 – Internat. Corrosion Conf. Series 2013.
298
- 299 [2] American Welding Society. Welding Handbook: Metals and Their Weldability. 9th ed.
300 Vol 4. Miami: American Welding Society; 2011, p. 307-8.
301
- 302 [3] Yan D, Drinkwater BW, Neild SA. Measurement of the ultrasonic nonlinearity of kissing
303 bonds in adhesive joints. NDT&E Int. 2009;42:459-466.
304
- 305 [4] Johnson PA. The new wave in acoustic testing. Mat. World 1999;7:544-6.
306
- 307 [5] Remillieux MC, Guyer RA, Payan C, Ulrich TJ. Decoupling Nonclassical Nonlinear
308 Behavior of Elastic Wave Type. Phys. Rev. Lett. 2016;116:115501.
309
- 310 [6] Van Den Abeele KEA, Carmeliet J, TenCate J, Johnson PA. Nonlinear Elastic Wave
311 Spectroscopy (NEWS) techniques to discern material damage. Part II: Single Mode
312 Nonlinear Resonance Acoustic Spectroscopy. Res. NonDest. Eval. 2000;12:31-43.
313
- 314 [7] Rivière J, Shokouhi P, Guyer RA, Johnson PA. A set of measures for the systematic
315 classification of the nonlinear elastic behavior of disparate rocks. J. Geophys. Res. Solid
316 Earth 2015;120:1587-1604.
317
- 318 [8] Ohtani T., Ishii Y. Nonlinear Resonant Ultrasound Spectroscopy (NRUS) applied to
319 fatigue damage evaluation in a pure copper. AIP Conf. Proc. 2012;1474:203.
320
- 321 [9] Ohtani T, Kusanagi Y, Ishii Y. Noncontact nonlinear resonant ultrasound spectroscopy to
322 evaluate creep damage in an austenitic stainless steel. AIP Conf. Proc. 2013;1511:1227.
323
- 324 [10] Payan C, Garnier V, Moysan J, Johnson P. Applying nonlinear resonant ultrasound
325 spectroscopy to improving thermal damage assessment. J. Acoust. Soc. Am.
326 2007;121(4):EL125-EL130.
327
- 328 [11] Payan C, Ulrich TJ, Le Bas P-Y, Saleh TA, Guimaraes M. Quantitative Linear and
329 Nonlinear Resonance Inspection Techniques and Analysis for material characterization:
330 Application to concrete thermal damage. J. Acoust. Soc. Am. 2014;136(2):537-46.
331
- 332 [12] Muller M, Sutin A, Guyer R, Talmant M, Laugier P, Johnson PA. Nonlinear resonant
333 ultrasound spectroscopy (NRUS) applied to damage assessment in bone. J. Acoust. Soc.
334 Am. 2005;118:3946-52.
335

- 336 [13] Ohara Y, Endo H, Mihara T, Yamanaka K. Ultrasonic measurement of closed stress
337 corrosion crack depth using subharmonic phased array. *Japanese J. Appl. Phys.*
338 2009;48(7S):07GD01.
339
- 340 [14] Ouchi A, Sugawara A, Ohara Y, Yamanaka K. Subharmonic phase array for crack
341 evaluation using surface acoustic wave. *Japanese J. Appl. Phys.* 2015;54(7S1):07HC05.
342
- 343 [15] Rivière J, Remillieux MC, Ohara Y, Anderson BE, Hauptert S, Ulrich TJ, Johnson PA.
344 Dynamic Acousto-Elasticity in a Fatigue-Cracked Sample. *J. Nondestruct. Eval.*
345 2014;33(2):216-25.
346
- 347 [16] Ohara Y, Anderson BE, Ulrich TJ, Le Bas P-Y, Johnson PA, Hauptert S. Localization of
348 closed cracks using multi-mode nonlinear resonant ultrasound spectroscopy. *J. Japanese*
349 *Soc. Nondest. Inspec.* 2015;64(12):571-8.
350
- 351 [17] Morlock F, Jacobs LJ, Kim J-Y, Singh P, Wall JJ. Nonlinear ultrasonic assessment of
352 stress corrosion cracking damage in sensitized 304 stainless steel. *AIP Conference*
353 *Proceedings* 2015;1650:1641.
354
- 355 [18] Anderson BE, Pieczonka L, Remillieux MC, Ulrich TJ, Le Bas P-Y. Stress corrosion
356 crack depth investigation using the time reversed elastic nonlinearity diagnostic. *J.*
357 *Acoust. Soc. Am.* 2017;141(1):EL76-EL81.
358
- 359 [19] Kundu T, Editor. *Nonlinear Ultrasonic and Vibro-Acoustical Techniques for*
360 *Nondestructive Evaluation*. 1st ed. Switzerland: Springer and ASA Press; 2018, chapters
361 2, 6, 10, 13, and 14.
362
- 363 [20] Kinsler LE, Frey AR, Coppens AB, Sanders JV. *Fundamentals of Acoustics*. 4th ed. New
364 York: Wiley; 2000, p. 68–87.
365
- 366 [21] Garrett SL. *Understanding Acoustics*. New York: Springer and ASA Press; 2017, p. 279-
367 305.
368
- 369 [22] Lott M, Remillieux MC, Le Bas P-Y, Ulrich TJ, Garnier V, Payan C. From local to
370 global measurements of nonclassical nonlinear elastic effects in geomaterials. *J. Acoust.*
371 *Soc. Am.* 2016;140(3):EL231-5.
372
- 373 [23] Jackson BK, Bosko DA, Cronin MT, Warwick JLW, Wall JJ. Detection of incipient
374 SCC damage in primary loop piping using fiber optic strain gages. *ASME Proceedings of*
375 *Pressure Vessels and Piping* 2014, 2014;PVP2014:28979.

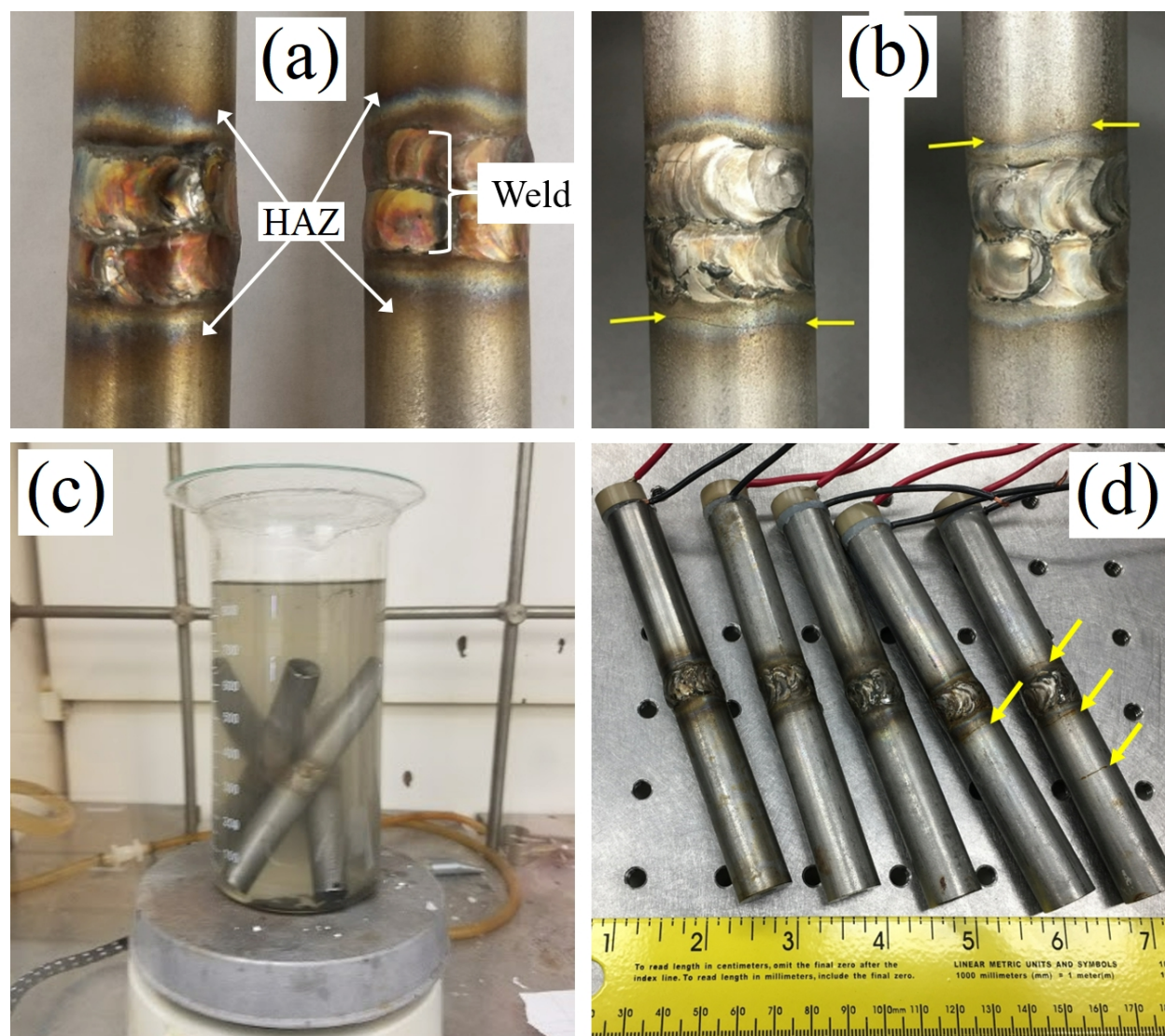
376 Table 1. Results given for experiments conducted on 13 samples. The quality factor and Young's
 377 modulus are measured during a low level excitation. There is a general increase in α_E as the days
 378 exposed to $MgCl_2$ increases.

379

Days Exposed	Quality Factor	Young's Modulus (GPa)	Max $\frac{\Delta f}{f_0}$ ($\times 10^{-3}$)	Max Strain ($\mu\epsilon$)	α_E	R
0	455	175	0.48	25.9	21.7	0.953
2	460	176	0.31	23.9	9.26	0.911
4	473	175	0.44	24.7	7.71	0.807
6	298	171	8.37	14.0	581	0.992
8	138	162	10.5	4.20	1690	0.999
10	294	162	5.56	11.6	3140	0.974
12	152	161	10.3	5.23	1970	0.997
14	182	163	21.5	6.50	2480	0.992
16	166	164	21.5	5.70	3710	0.994
18	234	158	22.1	6.50	2170	0.999
20	242	166	13.4	7.05	1960	0.938
22	74.6	149	33.2	2.51	10300	0.996
24	103	121	26.8	2.40	7500	0.977

380

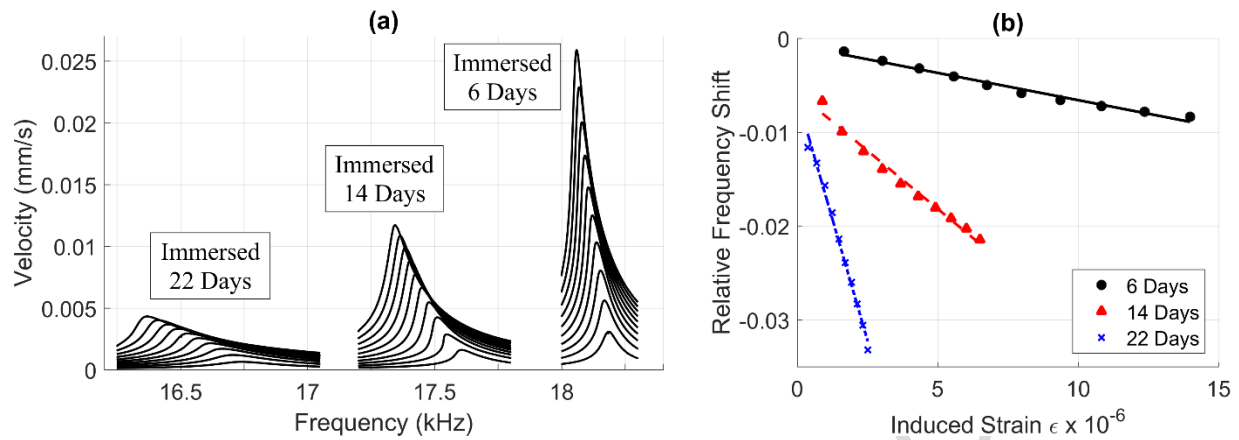
381



382

383 Fig. 1. (color online) (a) Close up photograph of 2 of the samples prior to exposure. Also
384 depicted are the weld region and the Heat Affected Zone (HAZ). (b) Close up photograph of 2 of
385 the damaged samples with cracks identified by arrows. (c) Photograph of some of the samples in
386 the hot magnesium chloride solution in a fume hood. (d) Photograph of five of the samples with
387 differing amounts of exposure and cracking (identified by the arrows).

388

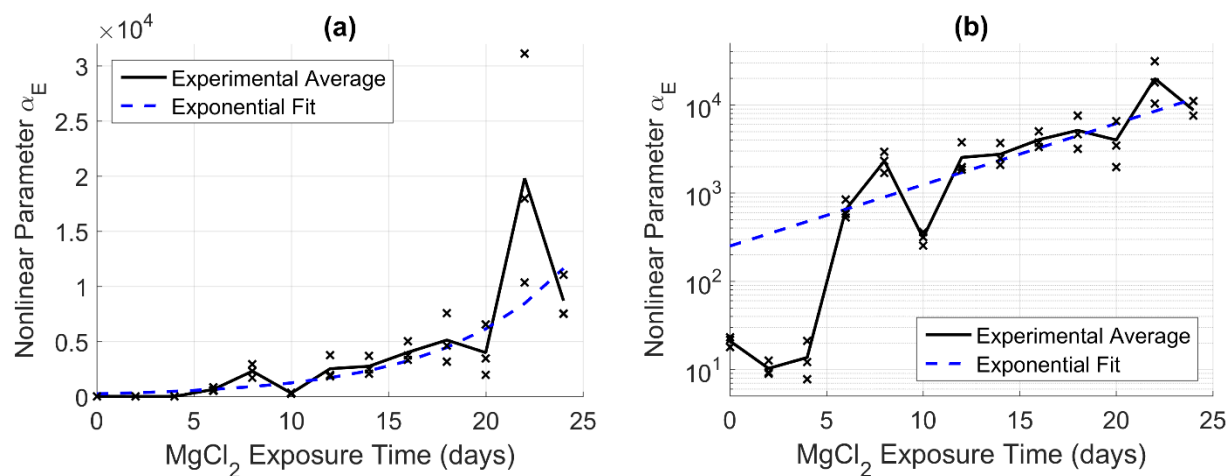


389

390 Fig. 2. (color online) (a) Sample nonlinear resonant ultrasound spectroscopy plots from three
391 samples exposed to hot magnesium chloride for 6, 14, and 22 days. (b) Relative frequency shift
392 as a function of induced strain, ϵ , for the three samples whose results were plotted in (a).

393 Included are trend lines which indicate the linear fits to the data.

394



395

396 Fig. 3. The measured nonlinearity parameter, α_E , as a function of exposure time for the samples

397 tested. (a) linear and (b) logarithmic scales. The “x” symbols represent each of three

398 measurements on each sample and the solid line represents their average values. The dashed line

399 represents the exponential fit of Eq. (4).

Highlights:

- Nonlinear Resonant Ultrasound Spectroscopy detects Stress Corrosion Cracking.
- Longer corrosion exposure leads to a greater shift in the resonance frequency.
- Nonlinearity appears to have an exponential dependence on exposure time.
- 304L stainless steel used here is the same as used in spent fuel storage canisters.